Nonlinear and quantum optics with liquid crystals

Svetlana G. Lukishova

E-mail: sluk@lle.rochester.edu

Abstract. Thermotropic liquid crystals' usual application is display technology. This paper describes experiments on light interaction with pure and doped liquid crystals under *for these materials unconventional* incident light powers: (1) under *high-power* laser irradiation, and (2) at *the single-photon level*. In (1), I will outline several nonlinear optical effects under *high-power, nanosecond laser irradiation* which should be taken into account in the design of lasers with liquid crystal components and in fabrication of optical power limiters based on liquid crystals: (1.1) athermal helical pitch dilation and unwinding of cholesteric mirrors (both in free space and inside laser resonators); (1.2) some pitfalls in measurements of refractive nonlinearity using z-scan technique under two-photon or linear absorption of liquids; (1.3) the first observation of thermal lens effects in liquid crystals under several-nanosecond, low-pulse-repetition rate (2–10 Hz) laser irradiation in the presence of two-photon absorption; (1.4) feedback-free kaleidoscope of patterns (hexagons, stripes, etc.) in dye-doped liquid crystals. In (2), at *the single-photon level*, it will be shown that with a proper selection of liquid crystals and a single-emitter dopant spectral range, liquid crystal structures can be used to control emitted *single* photons (both polarization and count rate). The application of the latter research is absolutely secure quantum communication with polarization coding of information. In particular, in (2.1), definite handedness, circular polarized cholesteric microcavity resonance in quantum dot fluorescence is reported. In (2.2), definite linear polarization of single (antibunched) photons from single-dye-molecules in planar-aligned nematic host is discussed. In (2.3), some results on photon antibunching from NV-color center in nanodiamond in liquid crystal host and circularly polarized fluorescence of definite handedness from nanocrystals doped with trivalent ions of rare-earths dispersed in liquid crystal host are presented.

Introduction

The development of liquid-crystal optics for high-power lasers began in 1979 at the Laboratory for Laser Energetics (LLE), University of Rochester, when it became apparent that some optical-component requirements of large-aperture solid-state lasers for thermonuclear fusion could not easily be met by solid-crystalline materials [1-3]. One such component, a high-quality, laser-beam apodized aperture has been the goal of solid-state laser fusion research programs both in the US and USSR since the early 1970's [1,4]. I worked at the Soviet/Russian Academy of Sciences (Moscow) on high-damage threshold apodized apertures and graded reflectivity mirrors [4-8] for reducing small-scale self-focusing effects [4,9] in high-power laser fusion systems and for improving the beam quality of industrial lasers [8]. To learn from the experience in *high-damage threshold* liquid crystal (LC) apodizing devices [1] and cholesteric mirrors [10-15], I visited LLE in 1993. Crucial in the preparation of LC materials with *high-damage threshold* under high-power laser irradiation is the purification of "as received" liquid crystals (LCs) through filtration to remove condensation centers for laser-induced bubble formation on the surface of the LC cell. It should be pointed out that high-power laser

applications of LCs are not the principal sector among all LC applications. Commercial vendors of LCs are therefore unlikely to provide materials optimized for high-power-laser use. That is why two types of possible contributors to laser damage of LC materials must be avoided. They are undissolved impurities that can be removed using particle filters and dissolved gaseous components that can be removed by degassing as well as synthesis byproducts or catalyst traces that can be removed by chromatography. In Refs. 1-3 it was shown that after purification of the "as received" LC samples the laser-damage threshold for massive material modification (visible burst of stable bubbles and glass chips in the cell surface and/or a web of scatter lines) improved sharply. For purified (using 0.2-μm particle filter) and degassed, isotropic 5CB, thresholds for permanent photolysis at ~ 9.6 J/cm^2 and ~ 4.4 J/cm^2 were observed under single and multiple shots respectively (1 ns pulse duration, 1-mm beam diameter, wavelength λ = 1.053 μm). Under similar conditions, transient-bubble "damage" observable under 110 x dark-field magnification in "as received" LCs occurred at ~ 0.76 J/cm^2 for isotropic 5CB and ~ 0.89 J/cm^2 for isotropic E7 (single-shot threshold) [1,3,16].

A similar problem in purification of "as received" LC materials arises when the LC is used as the host for single-emitters. In this case, single-photon counting detectors can detect fluorescence from impurities in the LC material itself [17] instead of fluorescence from a particular single emitter. In addition, for some types of single emitters it is desirable to avoid oxygen, the singlet-state of which can contribute to single-emitter bleaching. Removing the oxygen from a monomeric LC by saturation with helium or argon gas permitted us to record cw-excitation fluorescence from single dye molecules without bleaching for more than 1 hour [18,19].

The structure of this paper is as follows. It consists of two parts. Part 1 is an overview of my research on LCs under high-power laser irradiation. Chapter 1.1 of this part is devoted to my Moscow research at the Institute of the Radio Engineering and Electronics of the Russian Academy of Sciences on athermal cholesteric pitch dilation and unwinding of cholesteric liquid crystal (CLC) mirrors by the field of a light wave. Several groups tried to achieve this goal, but my group was the first who succeeded in it. These experiments were carried out both in free space and with the CLC mirror as the output coupler of a laser resonator. Special conditions of experiments permitted to prove that this effect is not connected with heating. I used purified CLC material provided by A.W. Schmid (LLE, University of Rochester). CLC mirrors were prepared by S.V. Belyaev's group of the Moscow Organic Intermediates and Dyes Institute NIOPIK. Two of my students of the Moscow Institute of Physics and Technology (FizTech), K. Lebedev and E. Magularia participated in this project. The research was supported by Grants of the International Science (Soros) Foundation, the Russian Government, and the Russian Foundation for Basic Research.

Chapter 1.2 is devoted to some of my results obtained at the Liquid Crystal Institute, Kent State University, on nonlinear absorption and refraction of cyanobiphenyl liquid crystals to high-power, several-nanosecond laser irradiation, using z-scan measurements. Two effects were observed under conditions of two-photon absorption: dependence of nonlinear refraction on laser-beam diameter (thermal-density nonlinearity) and the first-time observation of thermal-lens in LCs under several nanosecond irradiation and low-pulse-repetition rate. This work was made possible by the hospitality of P. Palffy-Muhoray and with the help of T. Kosa and B. Taheri.

Chapter 1.3 is devoted to feedback-free pattern formation using highly absorbing dye-doped nematic liquid crystals. This work was carried out at the Institute of Optics, University of Rochester, owing to the hospitality of R.W. Boyd and with the help of K. Marshall and N. Lepeshkin.

Part 2 of this paper describes my investigation, at the single-photon level, of LCs doped with single emitters (dye molecules, nanocrystal quantum dots, NV-color centers in nanodiamonds), and rare-earth doped nanocrystals. To my knowledge, this is the first research on LCs at the single-photon level. Chapter 2.1 describes the results on circularly polarized microcavity resonance in quantum dot fluorescence in a CLC host with 4.9 times intensity enhancement in comparison with polarization component of opposite handedness. Chapter 2.2 is devoted to a single-photon source with definite linear polarization using dye-doped nematic LC. Chapter 2.3 discusses using other type of emitters in liquid crystal hosts – nanodiamonds and nanocrystals doped with trivalent ions of rare-earths.

These projects supported by U.S. ARO and three NSF grants as well as Air Force and NASA graduate student fellowships, were carried out at the Institute of Optics, University of Rochester. My Ph.D. students L.J. Bissell [20] and J.M. Winkler as well as undergraduates C. Supranovich, R. Knox and summer research associate P. Freivald contributed to this project. I also used help and advice of K. Marshall, A.W. Schmid, L. Novotny, and A. Lieb. Some oligomeric CLC material was synthesized by S.-H. Chen's group, some nanocrystal quantum dots were synthesized by T. Krauss' group, nanocrystals with rare-earth ions were prepared at the University at Buffalo (Prasad's Institute for Lasers, Photonics, and Biophotonics). C.R. Stroud and R.W. Boyd contributed in discussions.

1. Liquid Crystals under High-Power Laser Irradiation

1.1. Athermal Cholesteric Pitch Dilation and Unwinding by the Field of a Light Wave

In 1982, Winful determined that athermal, light-induced changes in the pitch of the cholesteric helix lead to a reflectivity drop of a CLC mirror in the region of selective reflection [21]. However, later attempts [22,23] at detecting this effect in laser fields remained unsuccessful, in spite of the fact that chiral unwinding under the influence of both static and time-varying *electric* and *magnetic* fields had been observed. The challenge in observing *athermal* helix pitch dilation by *optical* fields arises from the larger than E ~ 10^4 V/cm electric-field strength requirement on the optical wave that needs to act on the CLC for time periods commensurate with the characteristic unwinding time of the helix t_h ~ several milliseconds. Therefore, neither short-pulse intensities [22,23] exceeding by an order of magnitude Winful's estimation nor rather low intensities applied cw [10-13], succeeded in triggering nonlinear changes in the reflectivity of nonabsorbing CLC mirrors. In reports [10-13], only changes in curvature and improvement of a beam profile of CLC mirrors were demonstrated in a cw-laser beam.

The first athermal drop in CLC mirror reflectivity in response to strong, circular polarized laser radiation was observed by my group in 1995 [24-28]. A special laser operating mode was selected using a pulsed, 4.5 kHz pulse-repetition-rate laser with an accumulation effect from many pulses. The effect was observed both in free space [24-25, 27-28] and inside a laser resonator [24,26,27-28] with a CLC mirror as the output coupler. To distinguish a field-induced orientational effect from thermal changes of the cholesteric pitch, the laser was switched to cw-operation with the same average intensity as in the pulsed regime. The effect was only observed at pulsed irradiation and depended only on peak intensity, but not on average intensity. The effect was demonstrated in four CLC mirrors with different substrate-surface-treatment methods for planar alignment. Sections of this Chapter 1.1 are devoted to the details of the experiments and their discussions.

It should be noted, that the authors of Ref. [29] also observed nonlinear selective reflection effects using the property of CLCs to achieve faster orientational response time to high-intensity beams. At incident, single-pulse peak intensities of ~ GW/cm^2, the CLC mirror reflectivity dropped even for single, nanosecond pulses. In paper [29], the light-induced reflectivity drop of CLC mirror was used in a Q-switched laser for passive cavity-dumping and an improved transverse beam profile.

1.1.1. Cholesteric mirrors in free space

For these experiments, we used a Nd:YAG laser with 1.064 μm wavelength. In this spectral region, *no two-photon absorption* effects in the CLC material should be observed. The laser operated in two regimes: (1) in cw mode and (2) in an acousto-optically Q-switched mode, emitting high-repetition-rate (4.5 kHz) pulse trains, each pulse being 500 ns long. In either mode, the average power reaching the CLC samples was between 0.3 and 1 W. Beam cross-sections before focus were monitored by a CID camera and video processing setup. From the recorded beam profiles, $1/e^2$ intensity beam diameters of between 50 and 200 μm were derived, corresponding to sample-plane peak-intensities (for 500-ns pulses) of 10^6-10^7 W/cm^2.

Upon focusing of free-space-propagating, 500-ns, 4.5-kHz-repetition-rate pulses into the CLC layer, we observed an increase in CLC-mirror transmittance of between 5% and 30-80%. This reflectivity drop appeared within 1 to 10 min from the onset of irradiation (Figure 1), depending on the

specific mirror. Interestingly, this effect did not depend on the magnitude of the average-intensity. Under cw irradiation conditions, we did not observe any effect even at average intensities twice as large as the average intensities in the pulsed, high-repetition rate mode. Furthermore, the effect appeared only, even in the case of high-repetition-rate pulse irradiation, under reflection of the incident light from the *strong-anchoring* side of the CLC mirror. Under 180° reversal, i.e., with the weak-anchoring side facing the incident beam, we did not observe any effect.

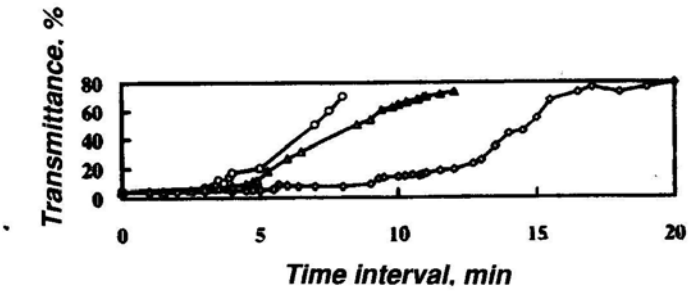

Figure 1. Dependence of a CLC mirror transmittance on irradiation time under high repetition rate, pulsed irradiation at different incident intensities.

The temperature drift in selective reflection for our given CLC mixture is estimated at +1 nm/C°, requiring a temperature excursion of more than 50 C° to account for the ~70% change in CLC-mirror transmittance at 1.064 μm. We did not observe such heating in the present CLC cells.

A recovery of the mirror reflectivity to its prior condition appeared after either terminating irradiation or switching it to cw-mode.

1.1.2. Cholesteric mirrors in laser resonators

For the laser-resonator studies, a plane-parallel cavity of the same laser used in section 1.1.1 was formed by a dielectric hard mirror and a CLC output coupler. An active Nd:YAG element was pumped by a continuously operating flashlamp filled with krypton (the voltage across this lamp was 100 V). Pumping of the active element generated a thermal lens whose optical power was +1 dioptre/kW. Switching to high pulse-repetition rate operation (500 ns pulse duration, 4.5 kHz pulse repetition rate) was performed by an acousto-optical switch. A quartz quarter waveplate was placed inside the resonator between the active element and the CLC output coupler. The diameter of the optical beam at the laser output was ~ 0.8 mm at an average output power of 1 W. No significant difference was observed between the slope efficiency of the laser with conventional dielectric or CLC output mirrors when the reflection coefficients were the same. The advantage of the CLC mirror was a lower sensitivity of the laser operation to cavity misalignment. At cw-operation and at low pumping rate in the pulsed high-repetition-rate regime, the slope efficiency and the lasing stability were the same for laser with CLC and dielectric mirrors. At high flashlamp currents, the average output power obtained in the high-repetition-rate mode decayed rapidly and disappeared after 0.5–5 min from switching, but only when the side of the CLC mirror with strong surface anchoring was facing the gain medium. The pump threshold (i.e., the current to the flashlamp) at which lasing was suppressed was different for each CLC mirror. It was 28.5–29.5 A for the output mirrors 1–3 with reflection coefficient R = 95%, and ~ 24.5 A for the CLC mirror 4 with R = 85%.

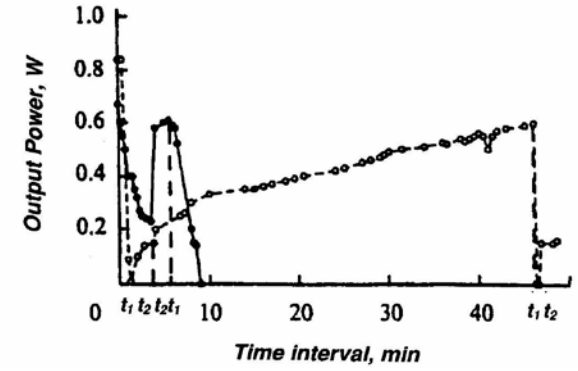

Figure 2. Time dependence of the average output power of a CLC mirror laser with changing the operating regime from cw to high-repetition rate (t_1) and back to (t_2). Solid and dashed curves present results for different mirrors.

Figure 2 depicts the time dependence of the laser output power obtained for two CLC mirrors when a change from the cw to the pulsed regime occurred at high flashlamp currents. Turning on the acousto-optical switch (at t_1) quenched the lasing action because of a drop in the reflection coefficient of the CLC mirror. Turning off the switch (at t_2) gradually restored the lasing action. A second change to the pulsed regime suppressed lasing again and it was restored when the laser was made to operate in the cw-mode again.

1.2. Thermal-Density Nonlinearity and Thermooptical Effects in Liquid Crystals under High-Power, Several Nanosecond Laser Irradiation

In this Chapter, I will briefly overview some of my results on nonlinear optical response of cyanobiphenyl LCs to high-power, nanosecond laser irradiation which I obtained at the Liquid Crystal Institute, Kent State University in 1997–1998. My full review on this subject including other group results is published in [28]. I would like to emphasize two important results which were overlooked in the past in z-scan measurements of LCs in the presence of nonlinear (or linear) absorption: (1) for isotropic LCs at several-nanosecond time scale and several tens-micrometers beam-waist-diameter the influence of coupled thermal and density effects on nonlinear refraction depends, through buildup time, on *the beam-waist diameter*; (2) for planar nematic layers, *cumulative effects* in heating (and in refractive nonlinearity) were observed even at low, 2–10 Hz pulse repetition rate, even for undoped (pure) liquid crystals. These results are important for optical power limiting and switching applications, and for intensity and beam-quality sensors of pulsed, high-power lasers.

Heating of undoped cyanobiphenyl LCs by short-pulse laser radiation in the visible range that drives photoacoustical (thermal-density) and thermooptical effects, is caused by two-photon absorption [30,31], concurrent or subsequent excited state absorption [30,32-34], and the efficient decay of the excited states through radiationless-recombination channels [30,32-34]. Strong nonlinear absorption in the visible was observed in optical power limiting studies of LCs [35-43] and in z-scan measurements [44-49]. For the nematic phase, the two-photon absorption coefficient has a several-times-higher value for incident polarization parallel to the LC molecular dipole direction than for perpendicular polarization [31].

As in any absorbing medium, in the presence of nonlinear absorption, the thermal mechanism causes refractive nonlinearity in nematic and isotropic LCs. The thermal nonlinearity coupled to density changes [35-36] (which is negative) competes with the orientational (positive) nonlinearity in changing the sign of the total refractive nonlinearity [28]. Another mechanism of density changes, electrostriction, with buildup time in the nanosecond range, is comparable to thermal/density contributions if medium absorption coefficients are low. At 0.532 μm a strong heating mechanism exists for the monomeric LCs as a result of two-photon and excited state absorption. That is why electrostriction is neglected in these experiments.

Refractive index changes by heating are the sum of two contributions:

$$\Delta n = (\partial n / \partial \rho)_T \Delta\rho + (\partial n / \partial T)_\rho \Delta T \quad , \qquad (1)$$

where ρ is the density, T is the temperature. It is very important in the current context that each term in (1) has its own turn-on time, and will contribute differently under transient and steady-state regimes [28,50-52].

1.2.1. Thermal-density nonlinearity ($(\partial n / \partial \rho)_T \Delta\rho$)

For several-nanosecond pulse duration and several tens of micrometers beam waist, the buildup time t_{ac} of the thermal-density nonlinearity ($\Delta n = (\partial n / \partial \rho)_T \Delta\rho$) can be close to the laser pulse duration t_o:

$$t_{ac} = r_o / V_s \quad , \qquad (2)$$

where r_o is the beam radius and V_S is the velocity of sound (V_S (LCs) ~ 1500 m/s). For $t_{ac} > t_o$ the thermal-density-nonlinearity will not develop during the pulse. Experimental values of nonlinear refractive index n_2 for this transient regime were reported in Ref. 50 for absorbing organic liquid. It was found experimentally, that the transient absolute value of n_2 for t_o = 5 ns diminishes with r_o

increasing from 9 to 32 μm. (The value of n_2 is defined in our paper by $n = n_0 + 1/2\ n_2|E|^2$). In a series of papers [51,52] numerical modeling was carried out for this regime. Acoustic grating generation in LCs have been intensively studied both under subpico-, pico- and nanosecond excitation [30,32-36].

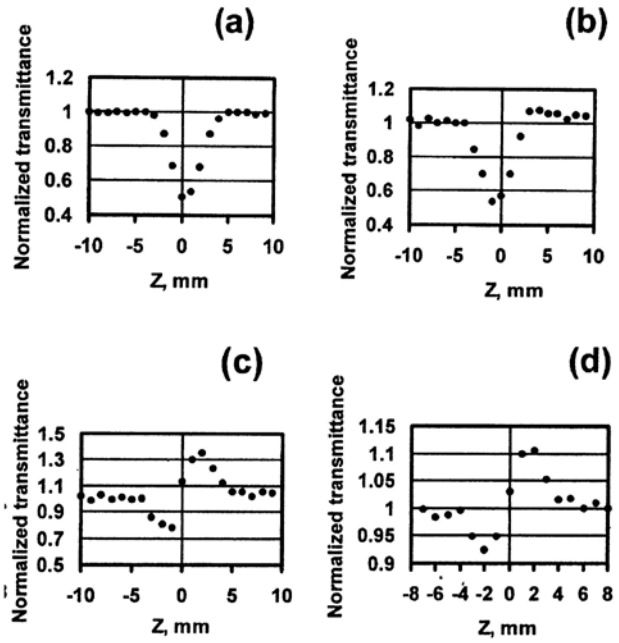

The typical z-scan curves of *transient* nonlinear refraction of room-temperature chiral additive CB15 samples with 2-mm thickness for 0.532 μm laser excitation [28,53] are presented in Figure 3 (a)-(c) for incident intensity I = 0.74 GW/cm^2. For comparison, a z-scan curve for CS_2 with 2-mm thickness is presented as well (Figure 3 (d)) for I = 0.73 GW/cm^2. The results from these curves yield the following values [28]: n_2(CB15) = 2.5 n_2 (CS_2). Beam-waist diameter was ~ 36 μm, and t_o = 6.8 ns, 10-Hz pulse repetition rate. The aperture factor for these z-scan measurements was S~0.1 [28].

Figure 3. Z-scan curves for chiral additive CB15: (a) open aperture; (b) closed aperture; (c) closed/open aperture; and (d) closed aperture for CS_2.

For 5CB above phase transition from nematic to isotropic state with 2-mm-cell thickness under similar conditions in the temperature interval 35.6–50°C, the *transient* value of n_2(5CB) varied from 2.5 to 3.7n_2(CS_2). In both cases, isotropic 5CB and CB15, self-focusing (converging lens) was observed. The absolute value of n_2(CS_2) for these conditions is equal to 1.2 x 10^{-11} esu [54]. In papers [44,49] for 7-μm diameter measurements, negative values of n_2 (self-defocusing) were reported for isotropic 5CB using the same laser. This difference is explained by the dependence of the value of transient thermal-density nonlinearity with negative sign on the beam-waist diameter. For 7-μm diameter, t_{ac} is less than the pulse duration time and nonlinear refraction as a result of density changes prevails under the positive-sign, transient, orientational nonlinearity. (5CB (nematic) and CB15 have identical chemical composition, but CB15, in difference to 5CB, contains a chiral carbon [28]).

1.2.2. Thermooptical effects $(\partial n/\partial T)_\rho \Delta T$ as the result of cumulative effects in heating of planar-aligned LC-cells

The thermooptic coefficient dn/dT in nematic LCs is extraordinarily large, ranking among the largest of all known materials [55]. Not unexpected for these highly anisotropic molecules, it depends on the orientation of the molecules. E.g., dn_{par}/dT was reported [56] of ~ 2.5 x 10^{-3} grad^{-1} for 5CB in the temperature interval 26–31°C for incident linear polarization parallel to the molecular orientation direction. For "perpendicular" polarization, dn_{perp}/dT is of opposite sign and equals ~ -1/2 dn_{par}/dT [55]. In the proximity of the phase transition to the isotropic state, the slope of both dn_{par}/dT and dn_{perp}/dT steepens [56].

For nematic LCs, it is well-known that the thermooptical effect experiences a lengthening of its buildup time (tens-hundreds of nanoseconds), rendering it insignificant on a several-nanosecond time scale [35,36]. Similar buildup times are reported in Ref. 50 for an absorbing organic fluid. Thermooptical effects for r_o = 32 μm were found to be more significant for pulses longer than ~100 ns.

Because of the slow buildup time, thermooptical (thermal-lens) spatial self-phase-modulation rings in the beam cross-section were observed only for cw laser radiation [57-59]. LC heating was in this case due to absorbing coatings on cell glass-substrates, dissolving absorbing dyes in LCs, and/or irradiation of unpurified LCs by high-average power (~ 1W for 100-μm spot size [57]) beams.

For pulsed lasers the first report on thermal-lens spatial self-phase-modulation rings was published in my papers [28,60,61]. I irradiated a planar-aligned nematic cell with a 0.532-μm laser beam (7 ns pulse duration, 10 Hz pulse repetition rate), propagating perpendicular to the cell walls. Linear polarization of the beam was parallel to the alignment direction of the LC molecules. In this configuration, no orientational effects should be observed. Over time spans of ~ 0.5–ten seconds high-contrast, concentric, elliptical diffraction rings appeared in the far-field (Figure 4) whose major axes orient themselves perpendicular to the incident polarization direction. Once formed, each set of rings may remain stable for up to several minutes. Upon continued pulsed irradiation over several minutes, the number of these rings varies systematically with laser intensity (sometimes between 1–2 and (up to) 20 rings). This ring pattern (see Figure. 4) differs from that typically obtained from orientational spatial self-phase modulation. In our case, the ring pattern evolves under polarization conditions for which, in principle, no orientational effects may occur (polarization of laser light is parallel to the director orientation). Under cw-irradiation at twice the average intensity than the average intensity under pulsed irradiation, the effect fails to exist.

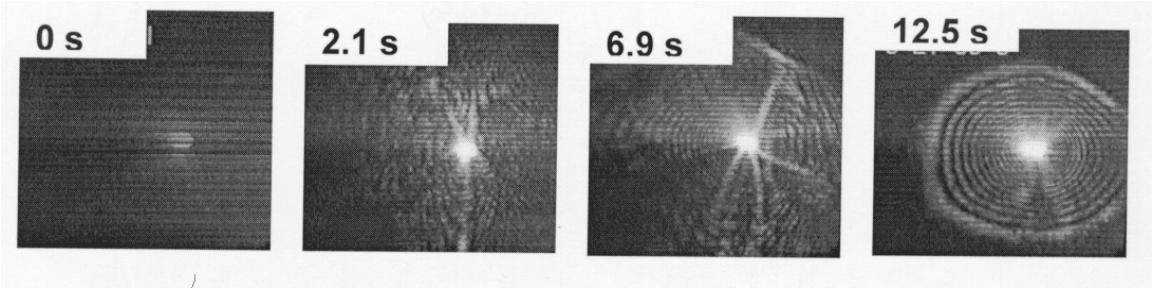

Figure 4. Time evolution of the elliptical ring pattern in the far-field (development of a thermal lens).

For explanation of the slow buildup time spatial self-phase modulation as well as its absence under cw irradiation of comparable average intensity, the heating of LC under *two-photon absorption* conditions was further scrutinized. The finite-element solutions were obtained by A.W. Schmid using the commercial ANSYS/Thermal code [28]. Numerical calculations of heating as cumulative action of many, 10-Hz repetition-rate pulses yield results on temperature increase and saturation at the end of the sequence. Evaluation of the phase shift caused in a laser beam by calculated temperature increase ($\Delta T \sim 5^{o}$C) gave number of self-modulation rings $N = 3$ [28]. A temperature increase after single pulse irradiation results in no diffraction rings in the beam. Only the cumulative action of many pulses approaching a steady-state value yields a stable spatial self-phase modulation elliptical ring pattern as displayed in Figure 4. It should be noted that some cumulative effects in LC nonlinearities at low pulse repetition rates were also reported in paper [63].

1.3. Feedback-Free Pattern Formation from Dye-Doped Liquid Crystals under Nanosecond Laser Irradiation

In this chapter, I will describe some experimental results on high-definition patterns observed under 10-Hz-pulse-repetition-rate, nanosecond laser irradiation of highly absorbing planar-nematic LC layers doped with dichroic dye. The patterns were observed at incident intensities $I \sim 5$–10 MW/cm^2 in a single beam and *without any feedback involved*. An incident polarization parallel to the nematic director was used. Under periodic pulsed laser irradiation, far-field beam patterns at the output of a dye-doped LC layer changed kaleidoscopically from rings and stripes to multiple hexagons. This pattern-formation regime had a buildup time of several seconds to minutes.

1.3.1. Experimental setup and cell preparation

A 0.532-μm laser beam with a pulse duration of ~ 20–26 ns and pulse repetition rate 10 Hz was focused by a 24-cm-focal-length lens into the dye-doped, planar-aligned nematic LC cell. The incident polarization was parallel to the orientation of the LC molecular director. The beam diameter in the focus was ~ 150 μm at the 1/e level [64]. The far-field patterns were recorded from a screen by a video camera onto magnetic tape from which the spatial intensity distribution for each pulse was digitized afterwards.

The nematic LC mixture E7 doped with the dichroic azodye "Oil Red O" with a 1.5% weight-concentration was used for filling the LC cells. E7 was supplied by EM-Industries (E7 is the mixture of cyanobiphenyls with ~51% of 5CB [28]); Oil Red O was supplied by Sigma-Aldrich. Planar-aligned nematic LC-layers were prepared using buffing techniques on Nylon 6/6 alignment layers on Soda-Lime-glass plates of size 2.5 cm x 2.5 cm x 0.3 cm. Glass-bead-spacers mixed with an UV-epoxy provided cell thicknesses between 10 and 20 μm. Coating the substrates by Nylon 6/6, buffing, cell assembly, and filling the cells with LC were carried out in a clean room. UV-cured epoxy was used for sealing the cells. Cell transmittance at low incident intensities was ~ 1% for an incident polarization parallel to the nematic director, and ~ 10–15 % for the perpendicular polarization.

1.3.2. Pattern formation experiments

At incident intensities I ~ 1–5 MW/cm^2 several phenomena were observed during repetitive illumination of LC-cells by a focused laser beam with 10-Hz pulse-repetition rate, for time periods of *several seconds* to *several minutes*. These phenomena include the following [65]:

- A polarization component *perpendicular* to the nematic director appeared after the beam passed through the nematic layer. Simultaneously, a several-fold increase in cell transmission was observed.
- Following that, *stable* far-field patterns appeared in the beam cross-section, possibly as the result of heat-flow [66,67] and/or flow-reorientational [67-71] birefringence (Figure 5):
    (1) The *perpendicular* polarization component (Figure 5, b) took on the far-field form of an optical four-leaf clover (Maltese-like cross). The bright axes of the cross were oriented at 45^o to the incident polarization;
    (2) The incident, *parallel* polarization component evolved into the far-field pattern in the form of a ring with a bright spot inside (Figure 5, c);
- *Stable* patterns existed for more than one hour of irradiation, but disappeared after switching the laser to a 5-Hz repetition rate.

At the higher-incident-intensities regime (I ~ 5–10 MW/cm^2), a new kind of high-definition patterns developed with a buildup time of several seconds to minutes and only for the polarization component *parallel* to the nematic director. Figure 6 shows the beam cross-sections of the two spatially separated polarization components both incident and induced (using a Glan-prism) overlapping in the center. The left side of the images depicts *the parallel-polarization* (incident) component; the right side – *the perpendicular-polarization* (induced) component. The optical four-leaf-clover of the *perpendicular-polarization* component (Figure 5, b) almost always became smeared into a random speckle pattern with a bright spot in the center (see the right side of the images). At the same time, *the parallel-polarization* component developed a high-definition pattern that kaleidoscopically changed from pulse to pulse from multiple hexagons (Figure 6, a), stripes (Figure 6, b), to rings (Figure 6, c) (see left sides of the Figure 6 images). The patterns disappeared after switching the laser to 5-Hz repetition rate. More details will be published elsewhere.

Near-field images of the laser-beam cross-section during the pulsed laser action showed kaleidoscopic changes from one to two and three spots patterns with dimensions ~ 5–15 μm and distance between spots ~ 35–70 μm.

The observation of high-definition hexagonal/stripes/rings patterns only for the "parallel" polarization component can be explained by the highly dichroic dye used for this experiment: cell transmittance was an order of magnitude higher for the "perpendicular" polarization component than

for the "parallel" polarization component. Hexagonal/stripes/rings patterns' low contrast makes them invisible for the "perpendicular" polarization component. Only a four-leaf-clover pattern can be seen in this component because of its existence's connection with another mechanism — the aberrations of the laser beam in heat-flow and/or flow-reorientational birefringent media.

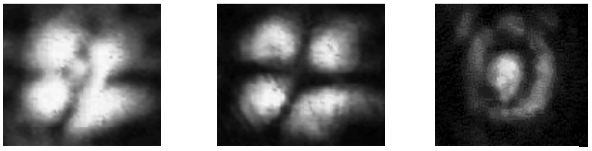

Figure 5. Far-field spatial patterns at low incident intensities: (a) no polarizer; (b) perpendicular-polarization (induced) component; (c) parallel (incident) polarization component.

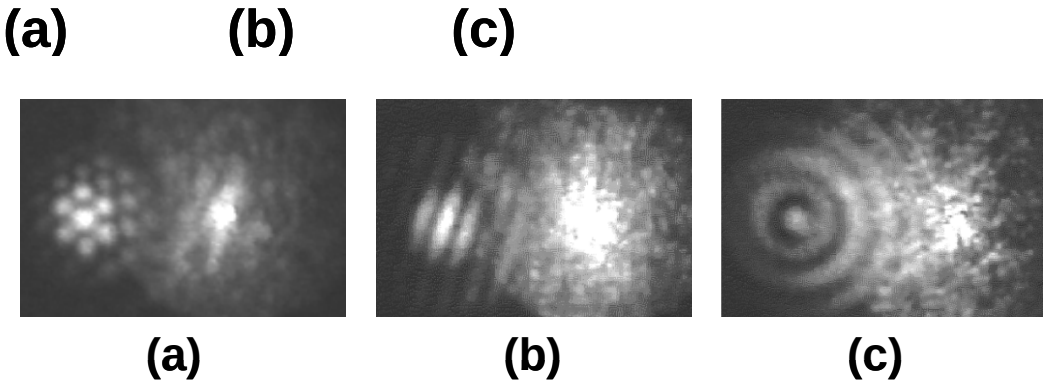

Figure 6. Representative selection of far-field spatial patterns at incident intensities ~5 – 10MW/cm^2 for the polarization component parallel to the director (left side of each image) and for the induced, perpendicular polarization component (right side of each image). A Glan prism was used to separate the two polarization components.

We explain the observed hexagonal/stripes/rings patterns in the far-field by the diffraction of the laser beam on light-induced one/two/three or more several-micron-size "drops" or "holes" with absorption and/or refraction properties different from the surrounding material. The patterns' ring structure can be attributed to the diffraction of laser light at the sharp boundary of the "drops". The variation in the "drop" numbers in the focal region, their size, the distance between them, and the gradient of transmittance inside the drop define the enormous variety of patterns we observed. A possible mechanism contributing to the creation of such "drops" is the instabilities in the presence of the Soret (thermal diffusion) effect, including phase separation of the dye from the liquid crystal. Phase separation of the dye from liquid crystal was also observed in Ref. 72 under cw-irradiation of a dye-doped liquid crystal.

2. Liquid Crystals at the Single-Photon Level

This chapter describes a new application for LCs — quantum information technology. A single-photon source (SPS) with definite polarization that efficiently produces photons exhibiting antibunching (separation of all photons in time) is a pivotal hardware element in absolutely secure quantum communication. For *single* photons, the second order correlation function $g^{(2)}(t) = \frac{< I(t)I(t+\tau) >}{< I(\tau) >^2}$ should have a minimum at $t = 0$ (in an ideal case $g^{(2)}(0) = 0$), indicating the absence of pairs, i.e., antibunching [73]. Here I is intensity. The critical issue in producing single photons exhibiting antibunching is the very low concentration of photon emitters dispersed in a host, such that, within an excitation-laser focal spot, only one emitter becomes excited which will emit only one photon at a time, because of its finite fluorescence lifetime.

In the BB84 quantum key distribution protocol, the sender (Alice) and receiver (Bob) employ the linear and circular polarization states of single photons. The linear and circular polarization bases can be used to provide two different quantum level representations of zero and one. So a desirable feature for a SPS is definite photon polarization, since, if the photon has unknown polarization, filtering it through a polarizer to produce the desired polarization for quantum key distribution will reduce by half the efficiency of a quantum cryptography system. In another implementation, a SPS becomes the key hardware element for quantum computers with linear optical elements and photodetectors [74].

In this chapter, experimental results of *room temperature*, robust SPSs with definite polarization using *single*-emitter fluorescence in either *cholesteric* or *nematic* LC hosts are discussed [17-20,75-79]. A desirable polarization state (either circular with definite handedness or linear with definite direction) of a fluorescence of the emitter in a LC host can be produced either by providing a chiral microcavity environment of CLC or by aligning emitters' dipole moments in a definite direction in a nematic LC. SPSs based on single emitters in LCs are the room-temperature alternatives to cryogenic SPSs based on semiconductor heterostructured quantum dots in microcavities prepared by molecular beam epitaxy (MBE), see review [80]. Definite linear polarization of single photons from heterostructured quantum dots both in elliptical pillar microcavities, and in a 2-D photonic crystal, was reported for resonance wavelength at *cryogenic* temperatures. In difference to expensive MBE, well developed LC alignment technology is relatively easy and fast. Different types of single emitters can be easily dissolved or dispersed both in monomeric (fluid-like) or oligomeric (solid) LCs. In addition to emitter alignment and the possibility of fabrication of photonic-bandgap structures from LCs, LC technology has another advantage. Special treatment of LCs (oxygen depletion) can protect the emitters from bleaching [18,19]. In Ref. [18,19], we reported on a significant diminishing of dye bleaching by saturation of LC with helium. Another remarkable advantage of LCs, e.g., changing its properties with temperature or by external-field variation, can provide SPS tunability. As single emitters, we used nanocrystal quantum dots (NQD), single NV-color centers in nanodiamonds, and single dye molecules.

The structure of this chapter is as follows. Section 2.1 describes antibunching and circularly polarized resonance with definite handedness in nanocrystal quantum dot fluorescence in a glassy CLC oligomer photonic bandgap microcavity. 4.9 times intensity enhancement was observed in comparison with a polarization component with opposite handedness. Section 2.2. is devoted to linearly polarized fluorescence with a definite polarization state from single dye molecules aligned in a glassy nematic LC oligomer. The last section 2.3. of this chapter describes photon antibunching from NV-color center in nanodiamond in liquid crystal host and circularly polarized fluorescence of definite handedness from nanocrystals doped with trivalent ions of rare-earths dispersed in liquid crystal host.

2.1. Circularly Polarized Microcavity Resonance in Quantum Dot Fluorescence in a Photonic Bandgap Cholesteric Liquid Crystal Host

We used left-handed cyclosiloxane oligomeric CLC powder from Wacker Chemie [81,82] and produced a planar-aligned glassy CLC structure doped with CdSeTe nanocrystal quantum dots (NQDs), Qdot 800 ITK organic, Invitrogen, fluorescence maximum at 790 nm [78]. Doping was accomplished by heating the CLC to ~135° C (the oligomer's melting temperature) and then mixing the melted CLC with quantum dots dispersed in toluene at a concentration of ~1 μM, with heating allowed to continue until the toluene evaporated. Subsequently, cells were prepared using two polyimide buffed glass coverslips. The CLC doped with quantum dots was placed on a buffed coverslip and heated beyond the oligomer clearing temperature of 180° C. After the sample was cooled to ~135° C, the second buffed coverslip was placed on the first and sheared along the direction of polyimide buffing. A slow cooling process back to a glassy (solid) state preserved the CLC order. This resulted in a photonic bandgap microcavity with a center wavelength of 910 nm.

Prepared samples were analyzed using our homemade confocal microscope setup. We excited the sample with cw, 633 nm laser light from a HeNe laser and observed the spectrum of the sample's

fluorescence. By placing an achromatic quarter waveplate and linear polarizer in front of the spectrometer, we were able to filter for different handedness of circularly polarized (CP) fluorescence.

The resulting fluorescence spectra can be seen in Figure 7, left. Left-handed (LH) CP light experienced the photonic bandgap and therefore the black LHCP curve in Figure 7, left (curve 1) shows microcavity resonance, indicating that the LHCP light coupled to the cavity mode. The LHCP fluorescence had a center wavelength of 833 nm and a FWHM of 16 nm (Q ~ 50), as compared to a FWHM of 76 nm for RHCP fluorescence. The center wavelength of this resonance roughly matches the edge of the photonic stopband, centered at 910 nm, and shown in Figure 7, left by the blue curve 3. The observed right-handed (RH) CP fluorescence is shown in red in Figure 7, left (curve 2) and was less intense due to not experiencing the CLC microcavity, showing no sign of line narrowing. The maximum intensity ratio between LHCP and RHCP was a factor of 4.9. To characterize the degree of circular polarization, the circular polarization dissymmetry factor g_e is used:

$$g_e = 2\,(I_L - I_R)/(I_L + I_R)\,, \qquad (3)$$

where I_L and I_R are intensities of LHCP and RHCP light, respectively. At the wavelength of the resonance shown in Figure 7, left, g_e = 1.3 [78]. Note that for unpolarized light, g_e = 0, which we observed when NQDs were spin-coated on a bare glass slip.

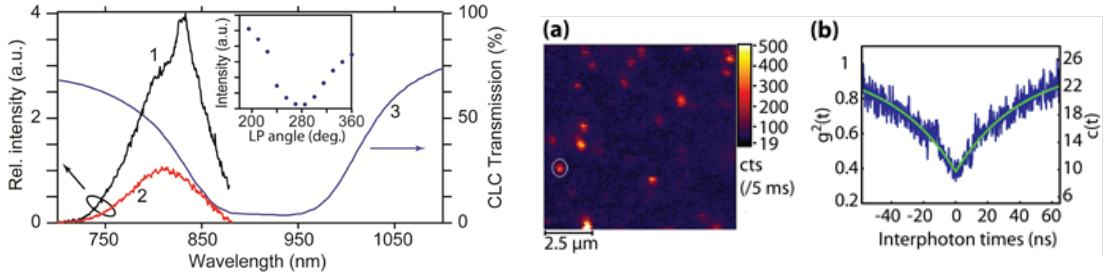

Figure 7, LEFT: Circularly-polarized fluorescence resonance from NQDs doped in a glassy CLC microcavity. Curve 1: LHCP fluorescence spectrum of the NQDs with a resonance at 833 nm. Curve 2: RHCP fluorescence spectrum for the same NQDs. Curve 3: selective transmission of LHCP light through CLC microcavity. Inset: Dependence of resonance peak intensity on rotation of a linear polarizer (LP) after a fixed quarter wave plate. RIGHT: (a) Confocal fluorescence microscopy image of single NQDs in a glassy CLC photonic bandgap microcavity. (b) Raw coincidence counts *c(t)* (right-hand scale) and $g^{(2)}(t)$ (left-hand scale), showing antibunching (dip at t = 0).

Figure 7, right (a), shows a confocal fluorescence raster scan taken of a sample prepared using a relatively low concentration of quantum dots dispersed in toluene (~10 nM), with the higher intensity spots indicating the location of fluorescing quantum dots in the glassy CLC microcavity. Focusing on a spot (circled in white on Figure 7, right (a)), we checked for photon antibunching and obtained the coincidence histogram shown in Figure 7, right (b).

Figure 7, right (b) displays the histogram of coincidence counts $c(t)$ in blue, with $g^{(2)}(t)$ derived by normalizing $c(t)$. The measured $g^{(2)}(0)$ value from the fit shown in Figure 7, right (b) (green, solid curve) is $g^{(2)}(0) = 0.382 \pm 0.037$ [78]. As $g^{(2)}(0) < 0.5$, this indicated that we have managed to isolate the fluorescence of a single quantum dot, serving as a source of antibunched light in a glassy CLC microcavity.

It should be mentioned that the same cholesteric structures can be used for lasing [83]. Our results on dye-doped cholesteric lasers are reported in Refs [84-85].

2.2. Single-Photon Sources with Linear Polarization

Another intriguing application of liquid crystals as hosts for single emitters is using the planar-alignment of nematic liquid crystals to provide doped molecular dipoles definite alignment along a preferred direction for efficient excitation [17,75]. This allows for the creation of a single-photon source with fluorescence of definite linear polarization.

Samples were prepared using $DiIC_{18}(3)$ dye (DiI) molecules from Molecular Probes doped in a glassy nematic liquid crystal oligomer synthesized by S. H. Chen's group of University of Rochester [17, 75]. Planar-aligned layers of this doped liquid crystal host of ~100 nm thickness were prepared using photoalignment of the liquid crystal molecules.

Photoalignment was performed by first spin-coating a Staralign-2100 linearly photopolymerizable polymer (Rolic Technologies Ltd.) to a cleaned cover glass slip, which was then cured at ~135° C. This film was then irradiated by a polarized UV light for 10 to 15 minutes, with further irradiation used to bleach the polymer impurity fluorescence.

An oligomer solution doped with dye and diluted in chloroform was subsequently spin-coated onto these Staralign coated glass slips. After the chloroform evaporated, we heated the sample to ~80°C, slightly above where the oligomer transition to a nematic state occurs, after which the sample was slowly cooled to a glassy state, preserving the planar-aligned nematic order.

To characterize prepared samples, we used the Witec alpha-SNOM in a confocal mode, exciting the sample using a Nd:YAG laser for cw, 532 nm irradiation. Single-photon counting avalanche photodiodes were used as photodetectors for confocal fluorescence scans, with a polarizing beamsplitter used so that each photodetector collected light of orthogonal polarization. Molecules were identified by the peak pixel intensity values and a linear polarization measure ρ was determined for each molecule by comparison of the perpendicular and parallel polarization images. Our measure of linear polarization was

$$\rho = (I_{par} - I_{perp}) / (I_{par} + I_{perp}), \quad (4)$$

where I_{par} and I_{perp} are, respectively, the fluorescence intensities parallel and perpendicular to the direction of alignment. The only difference of ρ with the degree of polarization is that it allows inclusion of the direction of polarization as part of the measure, depending on whether ρ is positive or negative.

The different ρ values that we found are histogrammed in Figure 8. A clear asymmetry in Figure 8 demonstrates a preference towards fluorescence polarized perpendicular to sample alignment. This is in contrast to the expected fluorescence from an unoriented sample, which would yield a symmetric ρ histogram [86].

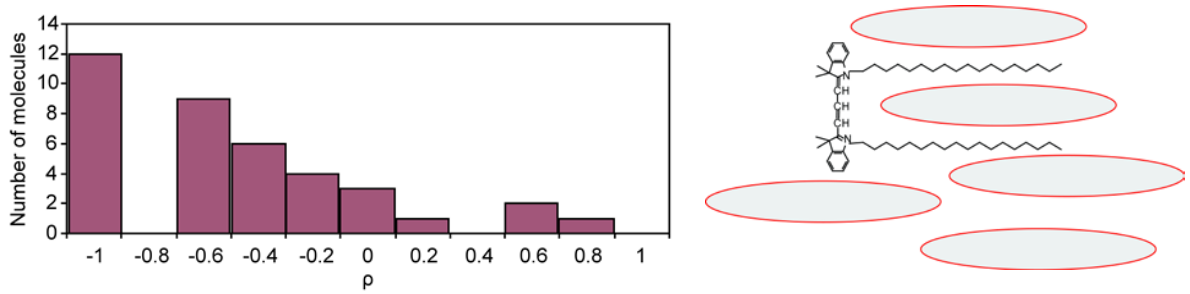

Figure 8. LEFT: Histogram of polarization measure ρ from 38 different DiI dye molecules in a planar-aligned nematic liquid crystal host [17,75]. RIGHT: Schematic view of a DiI dye molecule in a nematic liquid crystal host. The long axis (alkyl chains) of the DiI molecules tend to orient themselves along the rod-like nematic molecules, while the dipole, which is parallel to the bridge between the alkyl chains, orients perpendicular to the direction of liquid crystal alignment.

That DiI molecules doped in this planar-aligned liquid crystal host tend to fluoresce with polarization perpendicular to the alignment of the liquid crystal can be explained by the molecular structure of these molecules. As illustrated in Figure 8, right, it is likely that two alkyl chains orient themselves parallel to the rod-like molecules of the nematic liquid crystal host. The absorbing and emitting dipoles, however, are parallel to the bridge between these alkyl chains. Therefore, these

dipoles end up oriented perpendicular to the direction of liquid crystal alignment, hence the fluorescence having a polarization orthogonal to the alignment of the liquid crystal.

To confirm these results, additional experiments were carried out both with monomeric nematic liquid crystal and nematic glassy liquid crystal oligomers. Figure 9, left, shows intensity changes of fluorescence of DiI molecules in a planar-aligned monomeric nematic liquid crystal (E7), as the linear polarization of the excitation 532-nm laser beam was rotated over 360° degrees. Figure 9, left, shows a clear dependence of the fluorescence intensity on the exciting angle of polarization, where the maximum fluorescence occurred when the DiI molecules were excited by light with linear polarization perpendicular to the alignment of the liquid crystal.

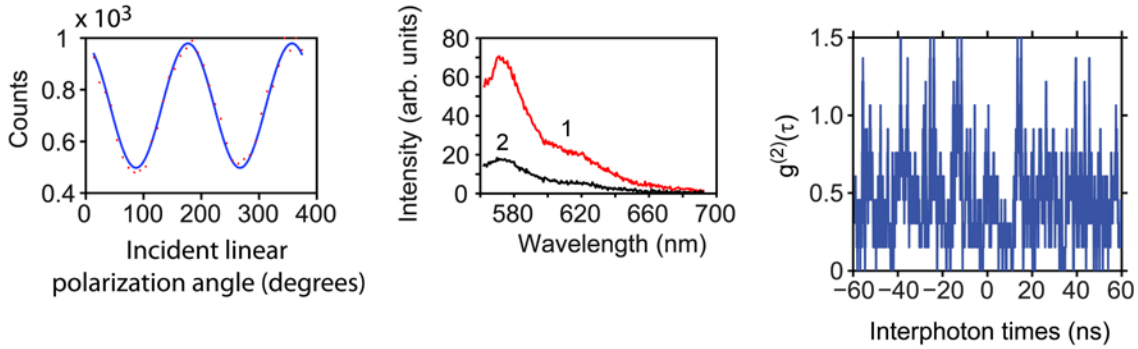

Figure 9. Polarized fluorescence of DiI dye in planar-aligned nematic liquid crystal hosts. Samples were excited using a 532 nm laser. LEFT: Intensity of DiI fluorescence in E7 as linear polarization of excitation laser light was rotated over 360°, with red dots showing experimental measurements and the blue solid curve providing a sinusoidal fit. The zero angle of polarization corresponds to the direction perpendicular to liquid crystal alignment. CENTER: Red (curve 1) and black (curve 2) show fluorescence spectrum with polarization perpendicular and parallel to the host alignment direction respectively. RIGHT: Antibunching histogram with a dip taken from the fluorescence of a single molecule of DiI dye in an E7 nematic host under pulsed, 532 nm excitation.

Figure 9, center, shows spectrofluorimeter measurements made for polarization perpendicular and parallel to the sample alignment, this time having used a sample of planar-aligned glassy nematic liquid crystal oligomer doped with DiI molecules of more than 1% concentration by weight. The value of ρ was measured from Figure 9, center, by comparing the peak intensities of the curves, yielding ρ = -0.5. The results of Figure 9, left and center, indicated a clear preference for fluorescence with definite linear polarization perpendicular to the sample alignment.

Figure 9, right, shows an antibunching histogram for a single molecule of DiI dye doped in an E7 nematic host, taken using pulsed, 532 nm excitation [20]. The value for $g^{(2)}(0)$ is $g^{(2)}(0) = 0.77 \pm 0.10$. This relatively high value of $g^{(2)}(0)$ may be due to the fact that the Raman spectrum of the E7 overlaps with the fluorescence spectrum of DiI dye.

2.3. Rare-Earth-Doped Nanocrystals and Color Centers in Nanodiamonds

Additional work with monomeric CLC based microcavities included doping with emitters such as nanodiamonds with nitrogen vacancy color centers and nanocrystals rare-earth ions. These alternative emitters can provide a source of single photons that is less likely to bleach.

Figure 10, left, shows photon antibunching from nitrogen vacancy color center in nanodiamond in a CLC (E7 and CB15) microcavity with a stopband centered at 725 nm, under cw, 514 nm excitation. The $g^{(2)}(0)$ value determined via fit (shown in Figure 10, left, as the dashed red line) was $g^{(2)}(0) = 0.74 \pm 0.08$. The fluorescence spectrum of nitrogen vacancy centers in nanodiamonds doped in this monomeric CLC when excited using cw, 514 nm excitation from an argon ion laser is shown in Figure 10, center.

A monomeric CLC microcavity made from a mixture of E7 and CB 15 was also doped with rare-earth Er^{3+} and Yb^{3+} ions in 20 nm to 30 nm sized $NaYF_4$ nanocrystals with 20% Yb and 2% Er. When these ions were excited using a cw, 976 nm diode laser at incident powers of ~500 μW, we were able to observe upconverted fluorescence of Er^{3+}, as shown in Figure 10, right. The emission lines observed were attributed to the transitions $^2H_{11/2}$, $^4S_{3/2} \rightarrow {}^4I_{15/2}$ (green) and $^4F_{9/2} \rightarrow {}^4I_{15/2}$ (red) of the Er^{3+} ions [87]. The populations of upper levels in Er^{3+}occur due to an efficient energy transfer from the Yb^{3+} to the Er^{3+}. This fluorescence was measured to have a circular polarization dissymmetry factor of g_e = -0.77 at 680 nm. These nanocrystals doped with rare-earth ions were prepared at the University at Buffalo (The Institute for Lasers, Photonics and Biophotonics).

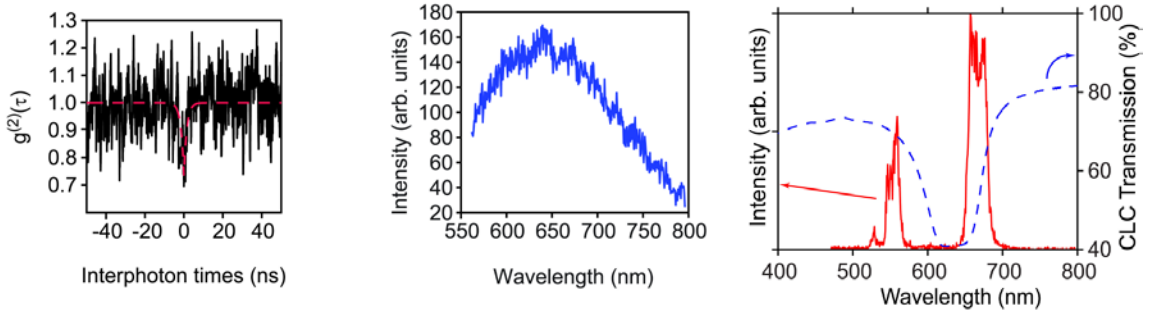

Figure 10. LEFT: Photon antibunching from nitrogen vacancy center nanodiamond in a CLC host. Black curve shows the raw data. Red dashed curve shows the fit. CENTER: Fluorescence spectrum of nitrogen vacancy centers in nanodiamonds in CLC host (cw, 514-nm laser excitation). RIGHT: Red solid lines: Fluorescence spectrum of Er^{3+} ions doped in $NaYF_4$ nanocrystals dispersed in a chiral CLC microcavity (E7 and CB15). The blue dashed curve shows the spectral transmission of CLC microcavity measured with unpolarized light.

Summary

An overview of some experiments and new applications of liquid crystals under two "extreme" levels of incident light powers are presented [79]. In many such applications for better device performance, "as received" liquid crystals materials must be purified and degassed. Several *nonlinear optical* effects under high-power, nanosecond laser irradiation are outlined: (1) athermal helical pitch dilation and unwinding of cholesteric mirrors by the field of a light wave; (2) dependence of refractive nonlinearity on the geometry of irradiation in the presence of two-photon (or linear) absorption; (3) the first observation of thermal lens effects in liquid crystals under several-nanosecond, low-pulse-repetition rate (2–10 Hz) laser irradiation in the presence of two-photon absorption; (4) feedback-free pattern kaleidoscope in dye-doped, highly absorbing liquid crystals.

At the single-photon level, definite linear and circular polarizations of single (antibunched) photons were obtained using single-emitter fluorescence in planar-aligned nematic and cholesteric hosts. Circular-polarized with definite handedness, cholesteric microcavity resonance was observed**.** These results are important for creation of room-temperature, single-photon sources, key devices for absolutely secure quantum communication. These single-photon sources can be used in fundamental *quantum optics* experiments.

Acknowledgement

The author acknowledge the support by the U.S. Army Research Office Award DAAD19-02-1-0285, National Science Foundation Awards ECS-0420888, DUE-0633621, DUE-0920500, and NASA NNX11AM82H Award. Research carried out in Russia was supported by the International Science Foundation Long-Term Award, Russian Government and Russian Foundation for Basic Research Awards.

The author thanks A.W. Schmid, S.V. Belyaev, V.F. Zolin, Ch.M. Briskina, V.M. Markushev, P. Palffy Muhoray, T. Kosa, B. Taheri, R. W. Boyd and his group members, L.J. Bissell, K. Marshal, L. Novotny and his group members, A. Lieb, J. Winkler, C.R. Stroud, S.-H. Chen and his group members, T. Krauss and his group members for help and/or support. These experiments were carried out in three institutions: the Institute of Radio Engineering and Electronics of the Russian Academy of Sciences, Moscow, Russia; the Liquid Crystal Institute (Kent State University), USA; the Institute of Optics, University of Rochester, USA. Some experiments were carried out at the liquid-crystal clean room and nanometrology facilities at the Laboratory for Laser Energetics, University of Rochester.

References

1. S. D. Jacobs, K. A. Cerqua, K. L. Marshal, A. W. Schmid, M. J. Guardalben and K. J. Skerrett, *JOSA. B* 5, 1962 (1988).
2. A. Schmid, S. Papernov, Z.-W Li, K. Marshal, T. Gunderman, J.-C. Lee, M. J. Guardalben and S. D. Jacobs, *Mol. Cryst. Liq. Cryst*. 207, 33 (1991).
3. S. D. Jacobs, K. L. Marshal and A. Schmid, in *Handbook of Laser Science and Technology, Supplement 2: Optical Materials*, ed. M. J. Weber (CRC Press, Boca Raton, FL, 1995), pp. 509-577.
4. S.G. Lukishova, Y.V. Senatsky, N.E. Bykovsky, A.S. Scheulin, Chapter 8, pp. 191-229, in *Self-focusing: Past and Present. Fundamentals and Prospects*, S.G. Lukishova, R.W. Boyd, Y.-R. Shen, Eds., Springer Series: Topics in Applied Physics, vol. 114, Springer NY, 2009, 605 p.
5. S.G. Lukishova, P.P. Pashinin, S.Kh. Batygov, V.A. Arkhangelskaya, A.E. Poletimov, A.S. Scheulin, B.M. Terentiev, *Laser and Particle Beams* 8, N 1-2, 349 (1990).
6. B.V. Gorshkov, V.K. Ivanchenko, V.K. Karpovich, I.K. Krasyuk, S.G. Lukishova, D.M. Margolin, P.P. Pashinin, EA. Simun, V.A. Sokolov, V.D. Terekhov, L.V. Chernysheva, *Kvantovaya Elektronika* 12, 1453 (1985). *Sov. J. Quant. Electron*. 15, 959 (1985).
7. S. G. Lukishova, N.R. Minhuey-Mendez, T.V. Tulajkova, *Kvantovaya Elektronika 21* 126 (1994). *Quant. Electron.* 24, 117 (1994).
8. S.G. Lukishova, S.A. Chetkin, N.V. Mettus, E.A. Magulariya, *Kvantovaya Elektronika* 23, 1040 (1996). *Quant. Electron*. 26, 1014 (1996).
9. S.G. Lukishova, R.W. Boyd, Y.-R. Shen, Preface, pp. V-XVIII, in *Self-focusing: Past and Present. Fundamentals and Prospects*, S.G. Lukishova, R.W. Boyd, Y.-R. Shen, Eds, Springer Series: Topics in Applied Physics, vol. 114, Springer NY, 2009, 605 p.
10. J.-C. Lee, S. D. Jacobs, T. Gunderman, A. Schmid, T. J. Kessler and M. D. Skeldon, *Opt. Lett*. 15, 959 (1990).
11. J.-C. Lee, S. D. Jacobs and R. J. Gingold, *Proc. SPIE* 824, 7 (1987).
12. J.-C. Lee, S. D. Jacobs and A. W. Schmid, *Mol. Cryst. Liq. Cryst.* 150b, 617 (1987).
13. J.-C. Lee, A. W. Schmid and S. D. Jacobs, *Mol. Cryst. Liq. Cryst*. 166, 253 (1989).
14. J.-C. Lee and S. D. Jacobs, J. Appl. Phys. 68, 6523 (1990).
15. J.-C. Lee, J. H. Kelly, D. L. Smith and S. D. Jacobs, IEEE J. Quant. Electron. 24, 2238 (1988).
16. A.W. Schmid, private communication.
17. S.G. Lukishova, A.W. Schmid, R.P. Knox, P. Freivald, A. McNamara, R.W. Boyd, C.R. Stroud, Jr., K.L. Marshall, *Molec. Cryst. Liq. Cryst*., 454, 1-14 (2006).
18. S.G. Lukishova, A.W. Schmid, A. J. McNamara, R.W. Boyd, and C.R. Stroud, *IEEE J. Select. Top. Quantum Electron.* 9, No 6, 1512 (2003).
19. S.G. Lukishova, A.W. Schmid, Ch. M. Supranowitz, N. Lippa, A. J. McNamara, R.W. Boyd, C.R. Stroud, Jr., *J. Mod. Opt*. 51, No 9-10, 1535 (2004).
20. L.J. Bissell, *Experimental Realization of Efficient, Room-Temperature Single-Photon Sources with Definite Circular and Linear Polarizations*, Ph.D. Thesis, University of Rochester, Rochester, NY (2011).
21. H. G. Winful, *Phys. Rev. Lett*. 49, 1179 (1982).

22. R. S. Becker, S. Chakravorti and S. Das, *J. Chem. Phys*. 90, 2802 (1989).
23. H. Espinet, M. Lesieski, M. Ramsburg and D. Jenkins, *J. Appl. Phys*. 59, 1386 (1986).
24. S. G. Lukishova, E. A.Magulariya and K. S. Lebedev, *Izvestiya Akademii Nauk Seriya Fizicheskaya* 59, 130 (1995). *Bulletin Russian Acad. Sci., Phys.* 59, 2086 (1995).
25. S. G. Lukishova, K. S. Lebedev, E. A. Magulariya, S. V. Belyaev, N. V. Malimonenko and A.W. Schmid, *JETP Lett*. 63, 423 (1996).
26. S. G. Lukishova, S. V. Belyaev, K. S. Lebedev, E. A. Magulariya, A. W. Schmid and N. V. Malimonenko, *Kvantovaya Elektronika* 23, 817 (1996). *Quantum Electron*. 26, 796 (1996).
27. S. G. Lukishova, S. V. Belyaev, K. S. Lebedev, E. A. Magulariya, A. W. Schmid and N. V. Malimonenko, *Mol. Cryst. Liq. Cryst*. 303, 79 (1997).
28. S.G. Lukishova, *J. Nonl. Opt. Phys. & Mater*. 9, N 3, 365 (2000).
29. D. Grebe, R. Macdonald and H. J. Eichler, *Mol. Cryst. Liq. Cryst*. 282, 309 (1996).
30. F. W. Deeg and M. D. Fayer, *J. Chem. Phys*. 91, 2269 (1989).
31. S. D. Durbin and Y. R. Shen, *Phys. Rev*. A 30, 1419 (1984).
32. R. Macdonald and H. E. Eichler, *Appl. Phys*. B 60, 543 (1995).
33. R. Macdonald and H. E. Eichler, in *The Optics of Thermotropic Liquid Crystals*, eds. S. Elston and R. Sambles (Taylor & Francis, London, 1998), 137
34. H. J. Eichler, R. Macdonald and B. Trosken, *Mol. Cryst. Liq. Cryst*. 231,1 (1993)
35. I.-C. Khoo, *Liquid Crystals, Physical Properties and Nonlinear Optical Phenomena* (John Wiley & Sons, New York, 1995).
36. I.-C. Khoo and S.-T. Wu, *Optics and Nonlinear Optics of Liquid Crystals* (World Scientifc, Singapore, 1993).
37. I. C. Khoo, *J. Nonlin. Opt. Mat*. 8, 305 (1999).
38. M. J. Soileau, E. W. Van Stryland, S. Guha, E. J. Sharp, G. L. Wood and J. L. W. Pohlmann, *Mol. Cryst. Liq. Cryst*. 143, 139 (1987).
39. M. J. Soileau, S. Guha,W. E.Williams, E.W. Van Stryland, H. Vanherzeele, J. L. W. Pohlmann, E. J. Sharp and G. Wood, *Mol. Cryst. Liq. Cryst*. 127, 321 (1985).
40. A. Hochbaum, J. L. Fergason and J. D. Buck, *Proc. SPIE* 1692, 96 (1992).
41. A. Hochbaum, Y. Y. Hsu and J. L. Fergason, *Proc. SPIE* 2229, 48 (1994).
42. K. McEwan and R. C. Hollins, *Proc. SPIE* 2229, 122 (1994).
43. K. J. McEwan and R. C. Hollins, *J. Nonlin. Opt. Phys. Mat*. 4, 245 (1995).
44. H. J. Yuan, L. Li and P. Palffy-Muhoray, *Mol. Cryst. Liq. Cryst*. 199, 223 (1991).
45. P. Palffy-Muhoray, H. J. Yuan, L. Li, M. A. Lee, J. R. DeSalvo, T. H. Wei, M. Sheik-Bahae, D. J. Hagan and E. W. Van Stryland, *Mol. Cryst. Liq. Cryst*. 207, 291 (1991).
46. T. Kosa, A. Dogariu, P. Palffy-Muhoray and E. W. Van Stryland, *Opt. Soc. Am. Tech. Dig. Ser*. 21, 57 (1995).
47. W. Zhao and P. Palffy-Muhoray, *Appl. Phys. Lett*. 65, 673 (1994).
48. 70. P. Palffy-Muhoray, T. Wei and W. Zhao, *Mol. Cryst. Liq. Cryst.* 251, 19 (1994)
49. L. Li, H. J. Yuan, G. Hu and P. Palffy-Muhoray, *Liq. Cryst*. 16, 703 (1994).
50. P. Brochard, V. Grolier-Mazza and R. Cabanel, *J. Opt. Soc. Am*. B14, 405 (1997).
51. D. I. Kovsh, S. Yang, D. J. Hagan and E. W. Van Stryland, *Appl. Opt*. 38, 5168 (1999).
52. D. I. Kovsh, D. J. Hagan and E. W. Van Stryland, *Opt. Express* 4, 315 (1999).
53. G. Lukishova, *Mol. Cryst. Liq. Cryst*. 331, 2469 (1999).
54. M. Sheik-Bahae, A. A. Said, T.-H. Wei, D. J. Hagan and E. W. Van Stryland, *IEEE J. Quantum Electron*. 26, 760 (1990)
55. P. Palffy-Muhoray, in *Liquid Crystals: Applications and Uses*, Ed. B. Bahadur (World Scientific, Singapore, 1990),Vol. 1, 493.
56. R. G. Horn, *J. Physique* 39, 105 (1978).

57. V. Volterra and E. Wiener-Avnear, *Opt. Comm*. 12, 194 (1974).
58. P. Wang, H. Zhang and J. Dai, *Opt. Lett*. 13, 479 (1988).
59. F. Bloisi, L. Vicari, F. Simoni, G. Cipparone and C. Umeton, *J. Opt. Soc. Am*. B5, 2462 (1988).
60. S. G. Lukishova, *Proc. SPIE* 3798, 128 (1999).
61. S. G. Lukishova, *Opt. Soc. Am. Tech. Dig. QELS'99*, 126 (1999).
62. M. Marinelli, F. Mercuri, U. Zammit and F. Scudieri, *Phys. Rev*. E 58, 5860 (1998).
63. C. Umeton, G. Cipparrone and F. Simoni, *Opt. Quantum Electron*. 18, 312 (1986).
64. S.G. Lukishova, N. Lepeshkin, R.W. Boyd, K. Marshall, *Molec. Cryst. Liq. Cryst*. 453, 393, 2006.
65. S.G. Lukishova, R.W. Boyd, N. Lepeshkin, and K.L. Marshal, *J. Nonl. Opt. Phys. & Mater*. 11, 341 (2002).
66. D. R. Baals and S. Hess, *Z. Naturforsch*. 40a, 3 (1985).
67. R. Elscher, R. Macdonald, H. J. Eichler, S. Hess and A. M. Sonnet, *Phys. Rev*. E 60, 1792 (1999).
68. I. C. Khoo, R. G. Lindquist, R. R. Michael, R. J. Mansfield and P. LoPresti, *J. Appl. Phys*. 69, 3853 (1991).
69. H. J. Eichler and R. Macdonald, *Phys. Rev. Lett*. 67, 2666 (1991).
70. R. S. Akopyan, B. Ya. Zel'dovich and N. V. Tabiryan, *Tech. Phys*. 38, 493 (1994).
71. C. Glorieux, K. A. Nelson, G. Hinze and M. D. Fayer, *J. Chem. Phys*. 116, 3384 (2002).
72. D. Voloschenko, D. and O. Lavrentovich, *J. Appl. Phys*. 86, 4843 (1999).
73. D. F. Walls and G. F. Milburn, *Quantum Optics*, Springer Verlag: Berlin, NY (1995).
74. E. Knill, R. Laflamme, G. J. Milburn, *Nature*, 409, 46 (2001).
75. S.G. Lukishova, A.W. Schmid, R. Knox, P. Freivald, L. Bissell, R.W. Boyd, C.R. Stroud, Jr, K.L. Marshall, *J. Mod. Opt*. 54, iss. 2 & 3, 417 (2007).
76. S.G. Lukishova, L. J. Bissell, V.M. Menon, N. Valappil, M.A. Hahn, C.M. Evans, B, Zimmerman, T.D. Krauss, C. R. Stroud, Jr., R.W. Boyd, *J. Mod. Opt.* 56, is 2 & 3, 167 (2009).
77. S.G. Lukishova, L.J. Bissell, C. R. Stroud, Jr., R.W. Boyd, *Optics and Spectroscopy*, 108, 417 (2010).
78. S.G. Lukishova, L.J. Bissell, J. Winkler and C.R. Stroud, *Opt. Lett*. 37, 1259 (2012).
79. S.G. Lukishova, *Mol. Cryst. Liq. Cryst*. 559, 127–57 (2012).
80. Y. Yamamoto, Ch. Santori, J. Vuskovic, D. Fattal, E. Waks, E. Diamanti, *Progr. Informatics* 2005, 1, 5 (2005).
81. T.J. Bunning and F.-H. Kreuzer F-H., *Trends Polym. Sci*. 3, 318 (1995).
82. S.G. Lukishova and A.W. Schmid, *Molec. Cryst. Liq. Cryst*. 454, 15-21 (2006).
83. H. Coles and S. Morris, *Nature Photonics* 4, 678 (2010).
84. K. Dolgaleva, S. K. H. Wei, S.G. Lukishova, S.-H. Chen, K. Schwertz, R.W. Boyd *JOSA B* 25, 1496 (2008).
85. S. K .H. Wei, S. H. Chen, K. Dolgaleva, S. G. Lukishova, and R. W. Boyd, *Appl. Phys. Lett.* 94, 041111 (2009).
86. H. Huang, A. Dorn, V. Bulovic and M. Bawendi, *Appl. Phys. Lett*. 90, 023110 (2007).
87. Z. Wang, F. Tao, W. Cai, L. Yao and X. Li, *Solid State Commun*. 144, 255 (2007).